International Journal of Dental Research and Allied Sciences
2022, Volume 2, Issue 1, Page No: 20-32

Available online at: www.tsdp.net

ISSN: 3062-3502

Original Article

Molecular Characterization of Granular Cell Tumors and Oral Cavity Schwannomas

Ana Souza[1], Pedro Lima[2], Juliana Costa[1,2]*

[1]Department of Oral Medicine (Oral Pathology), Dental School, Federal University of Goiás, Goiânia-Goiás, CEP 74605-220, Brazil.
[2]Department of Oral Medicine Dental, Association of Cancer of Combat of Goiás, Araujo Jorge Hospital, Goiânia, Brazil.

***E-mail** ✉ juliana.costa07@hotmail.com

Received: 08 November 2021; **Revised:** 21 February 2022; **Accepted:**23 February 2022

ABSTRACT

Granular cell tumours (GCTs) are infrequent submucosal growths, presumed to arise from Schwann cells, distinguished by large polygonal cells containing numerous lysosomes. This study sought to explore whether GCTs display features of antigen-presenting cells (APCs) or neural crest cells (NCCs) using immunohistochemistry and to contrast their expression patterns with Schwannomas. Expression of APC-associated markers (CD68, HLA-DR, CD163, CD40, CD11c) and NCC-associated markers (S100, SOX10, NSE, GAP43) was analyzed in 23 GCTs and 10 Schwannomas. Furthermore, RT-qPCR was conducted on 6 GCT cases to assess a possible NCC developmental signature. GAP43 emerged as a novel NCC marker for GCTs, while CD68 and HLA-DR staining provided limited support for an APC-like profile. RT-qPCR did not detect an NCC developmental program in GCTs, likely due to technical constraints.

Keywords: APC markers, Granular cell tumour, Immunohistochemistry, Schwannoma, Neural crest markers, RT-PCR

How to Cite This Article: Souza A, Lima P, Costa J. Molecular Characterization of Granular Cell Tumors and Oral Cavity Schwannomas. Int J Dent Res Allied Sci. 2022;2(1):20-32. https://doi.org/10.51847/y61zW2l2Ux

Introduction

Granular cell tumours (GCTs) are uncommon soft tissue lesions whose origin has been widely debated, with current evidence suggesting derivation from neural crest cells, particularly Schwann cells, based largely on immunohistochemical similarities with schwannomas. Typically, GCTs present as solitary benign growths, though multifocal and malignant forms have been reported [1]. Around half of all cases occur in the head and neck region, most frequently on the tongue, accounting for 23%–28% of all GCTs and 65%–85% of intraoral cases [1], with Allon *et al.* reporting that GCTs constitute 9.6% of benign oral mucosal tumours [2]. They generally appear in individuals in their fourth to sixth decades, with a female-to-male ratio of approximately 2:1 [3], and multiple lesions are observed in 2–10% of patients [4]. GCTs are slow-growing, painless sub-epithelial nodules that are firm and round [5]. In the oral cavity, lesions typically measure around 2 cm at diagnosis, with most being treated before reaching 3 cm [1]. Imaging is often non-specific, and larger lesions may mimic invasive growths on CT or MRI scans [6], while tumours exceeding 5 cm raise suspicion for malignancy [7]. Surgical excision with narrow margins is the standard treatment, and recurrence occurs in roughly 20% of incompletely excised cases and 2–8% of lesions with clear margins, likely due to residual satellite cells or tumour extensions [8, 9].

Macroscopically, GCTs appear as tan to pale, rubbery nodules lacking a capsule. Histologically, they consist of large polygonal or lozenge-shaped cells with abundant eosinophilic cytoplasmic granules and small eccentric nuclei. These granules are PAS-positive, diastase-resistant [10], and stain with Luxol fast blue

[1]. Cells are arranged in sheets or clusters, separated by thin connective tissue bands, with poorly defined tumour margins that may blend with overlying epithelium or underlying skeletal muscle, giving an infiltrative appearance. Detached clusters of cells, likely representing extensions rather than independent lesions, are often present [1]. Small nerves at the tumour periphery suggest a relationship with perineural cells, possibly linked to axonal injury [1]. Pseudoepitheliomatous hyperplasia is seen in nearly 50% of cases, which may be misinterpreted as squamous cell carcinoma (SCC) due to the rarity of GCTs and the relatively high frequency of SCC [11, 12].

GCTs were initially described by Weber and Virchow in 1854 [6], and Abrikossoff later proposed a myogenic origin, coining the term myoblastoma [1]. Subsequent electron microscopy and immunohistochemical studies excluded myogenic differentiation and suggested alternative origins, including histiocytic lineage, a common precursor with schwannomas, or undifferentiated mesenchymal fibroblast precursors that had phagocytosed cellular debris [13–17]. Several investigations have supported differentiation from neural sheath cells [9, 16–19].

In addition to evidence supporting a neural origin, some studies have proposed an endomesenchymal derivation for GCTs. Gurzu reported that GCTs express macrosialin (CD68), CD117 (c-kit), and RET [9]. Other studies have identified expression of CD63, LC3 (microtubule-associated protein 1 light chain 3, a marker of autophagy), and the antigen-presenting cell (APC) marker HLA-DR in GCTs [20–22], with HLA-DR and CD68 immunoreactivity indicating a potential APC phenotype. Pareja *et al*. recently described inactivating mutations in ATP6AP1 and ATP6AP2, genes involved in endosome acidification, in 72% of GCTs, suggesting that altered endosomal function may modify cellular signaling and confer oncogenic properties, further supporting a link to an APC-like phenotype [23]. Despite these findings, it remains unclear whether GCTs represent true neoplasms or reactive lesions based on current immunohistochemical evidence.

Proteins such as HLA-DR, CD68, CD163, CD40, and CD11c are characteristic of APCs and are involved in their functional activities [24–31], whereas S100, SOX10, NSE, and GAP43 are typically associated with neural tissues, neural-derived tumours, and neural crest–derived cells [32–36]. Growth-associated protein 43 (GAP43, also known as neuromodulin) plays a crucial role in axonal guidance, neural cytoskeleton organization, neurite growth, and synapse formation following nerve injury [35]. To date, GAP43 expression in GCTs has not been reported.

This study aimed to distinguish between an APC phenotype and a neural tissue phenotype in GCTs using immunohistochemistry (HLA-DR, CD68, CD163, CD40, and CD11c for APC markers) and polymerase chain reaction techniques, while comparing expression patterns with schwannomas. RT-qPCR was performed to assess RNA expression of nestin, SOX2, SOX9, SOX10, NF2, beta tubulin-III, and glial fibrillary acidic protein (GFAP)—proteins variably expressed in neural-crest-derived tissues and Schwann cells—alongside CD68, beta tubulin-3 (a neural tissue marker), and beta-actin as a control [37–43].

Results and Discussion

Demographics

The mean age of patients with biopsy-confirmed GCTs was 41.4 ± 13.1 years, with most cases occurring in the fourth to sixth decades: six cases in the fourth and fifth decades and seven in the sixth decade. In contrast, patients with schwannomas had a mean age of 25 ± 9 years, with the highest incidence in the third decade. Among GCT cases, 14 were female and 9 male, resulting in a female-to-male ratio of 1.56:1, while schwannomas showed a male predominance (8 males, 2 females; male-to-female ratio 4:1). The dorsal tongue was the most frequent site for GCTs (16/23 lesions, 69.5%). Lesion sizes ranged from 5 to 20 mm, with a mean diameter of 10.1 mm. All GCTs were managed with excisional biopsy, and although many cases had positive deep margins, no recurrences or relapses were observed. Schwannomas showed no clear site predilection **(Table 1)**.

Table 1. Demographics and site of biopsy.

Granular Cell Tumours			
Case No.	**Age**	**Sex**	**Site**
1	41	Female	midright dorsum of tongue
2	33	Female	dorsum of tongue
3	15	Female	dorsum of tongue
4	43	Male	dorsum of tongue

5	20	female	right tongue
6	36	Male	dorsum of tongue
7	48	female	left posterior hard palate
8	50	Male	dorsum of tongue
9	37	female	left lateral border of tongue
10	55	female	right palatal mucosa
11	39	female	dorsum of tongue
12	21	female	right dorsum of tongue
13	52	male	right lateral border of tongue
14	48	male	right dorsum of tongue
15	46	male	right dorsum of tongue
16	35	female	right dorsum of tongue
17	63	female	left dorsum of tongue
18	55	female	left dorsum of tongue
19	37	male	dorsum of tongue
20	21	female	right lateral border of tongue
21	56	male	dorsum of tongue
22	58	male	right lateral ventral tongue
23	43	Female	left dorsal tongue
Schwannomas			
Case No.	**Age**	**Sex**	**Site**
1	28	Male	buccal mucosa 37
2	21	Male	left dorsum of tongue
3	23	Male	right tip of tongue
4	41	Male	left buccal mucosa
5	16	Female	*** oral cavity
6	37	Female	lower lip mucosa
7	22	Male	lower lip mucosa
8	15	Male	left buccal vestibule
9	16	Male	dorsum of tongue
10	31	Male	Upper lip

*** Site of biopsy was unspecified, anatomically from the oral cavity.

Immunohistochemistry

The outcomes of the immunohistochemical analyses are presented in **Figures 1 and 2**.

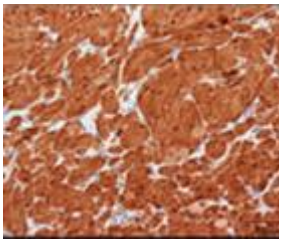

a)

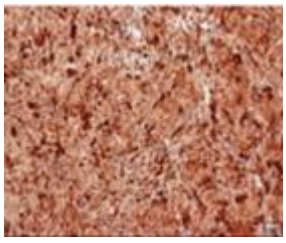

b)

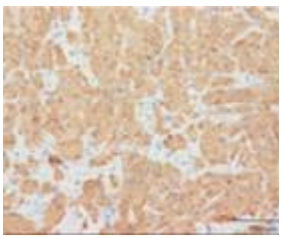

c)

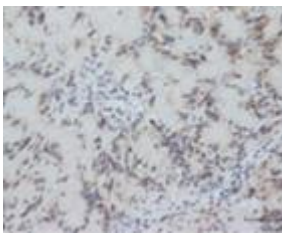

d)

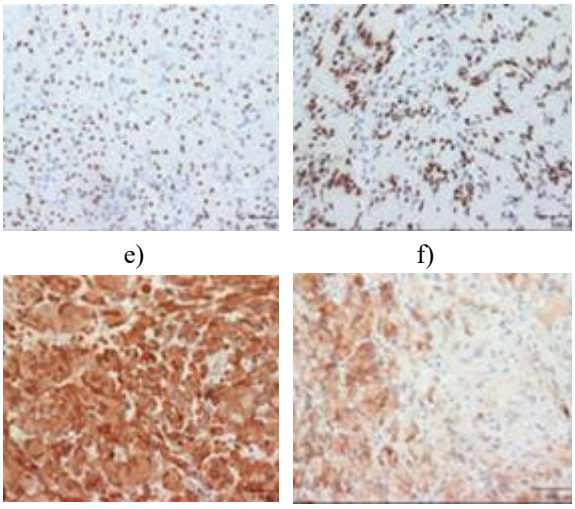

Figure 1. Immunohistochemical expression of neural markers in GCTs and Schwannomas, visualized using DAB (brown staining). Images were captured at 200× magnification, with a 100 µm scale bar indicating relative size. (A) S100 in GCT; (B) S100 in Schwannoma; (C) NSE in GCT; (D) NSE in Schwannoma; (E) SOX10 in GCT; (F) SOX10 in Schwannoma; (G) GAP43 in GCT; (H) GAP43 in Schwannoma.

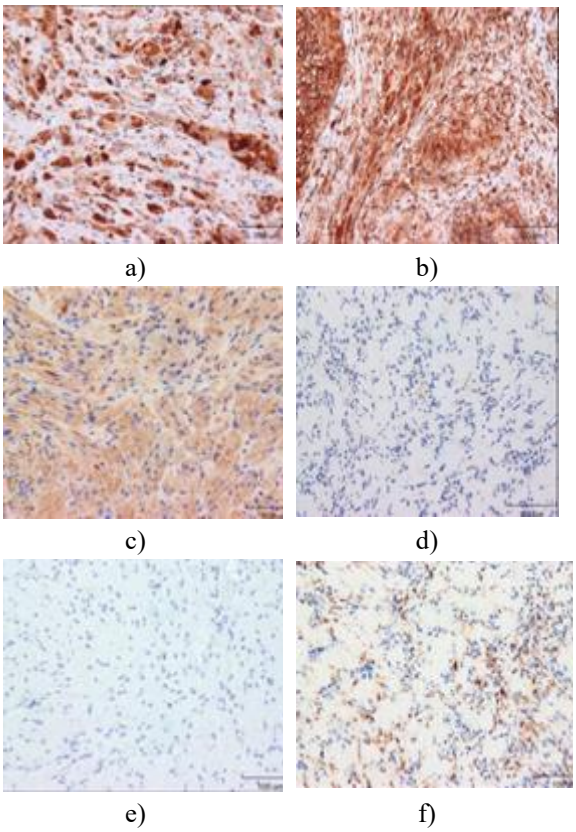

Figure 2. Immunohistochemical expression of antigen-presenting cell (APC) markers in GCTs and Schwannomas, visualized using DAB (brown staining). Images were captured at 200× magnification. (A) HLA-DR in GCT; (B) HLA-DR in Schwannoma; (C) CD68 in GCT; (D) CD68 in Schwannoma; (E) CD163 in GCT; (F) CD163 in Schwannoma.

S100 staining: S100 immunoreactivity was observed in both the cytoplasm and nuclei of GCTs and Schwannomas, with nuclear staining generally stronger than cytoplasmic staining. In Schwannoma spindle cells, staining was punctate with bands of higher intensity near the nucleus, while GCT cytoplasmic staining appeared more diffuse. Nearly all granular cells in GCTs and spindle cells in Schwannomas were positive, showing minimal variability in intensity **(Figures 1a and 1b)**.

NSE: In GCTs, NSE staining was confined to the cytoplasm, whereas Schwannomas exhibited predominantly cytoplasmic staining with some nuclear positivity in many cells. Nearly all granular cells of GCTs showed strong staining, while more than 50% of Schwannoma spindle cells were positive **(Figures 1c and 1d)**.

SOX10: SOX10 staining was exclusively nuclear in both GCTs and Schwannomas, with high intensity in all cells **(Figures 1e and 1f)**.

GAP43: GAP43 immunoreactivity was cytoplasmic in both tumours. In GCTs, two distinct staining patterns were observed: diffuse with sparse punctate staining or predominantly punctate with minimal diffuse cytoplasmic staining. Within a section, granular cells typically displayed one pattern over the other. Schwannomas differed markedly, showing diffuse cytoplasmic staining in all positive spindle cells, without a punctate pattern. Antoni A areas exhibited strong staining, while Antoni B areas showed weak or absent staining in fewer than 50% of cells, producing a patchy appearance **(Figures 1g and 1h)**.

HLA-DR: Both GCTs and Schwannomas displayed similar HLA-DR staining, primarily cytoplasmic with occasional nuclear positivity in GCTs. Staining was punctate over a diffuse background, with nearly all cells showing high intensity and minimal variability **(Figures 2a and 2b)**.

CD68: CD68 staining was cytoplasmic in both tumour types. GCT cells exhibited light, diffuse punctate staining, while Schwannoma staining varied: one case showed no appreciable staining, and the remaining nine cases had low to moderate intensity **(Figures 2c and 2d)**.

CD163: Schwannomas were positive for CD163 with strong punctate cytoplasmic staining in all sections, whereas GCTs were negative **(Figures 2e and 2f)**.

CD40 and CD11c: Neither GCTs nor Schwannomas showed immunoreactivity for CD40 or CD11c.

Semiquantitative analysis: **Table 2** summarizes cumulative scores for the percentage of cells stained and staining intensity in both GCTs and Schwannomas. A contingency table was constructed using percentage of cells stained (x-variable) and staining intensity (y-variable), followed by a linear-by-linear association test. The p-value ($<2 \times 10^{-16}$) indicated a near-perfect correlation between the two variables, leading to rejection of the null hypothesis of no association. Based on this correlation, subsequent analyses focused on staining intensity, which could be extrapolated to the percentage of cells stained.

Table 2. Mean DAB stain intensity and percentage of cells staining in GCTs and schwannomas.

IHC Antibody		Absent	Low	Medium	High	0 (0%)	1 (>0≤50%)	2 (>50%)
S100	GCT	-	-	-	23	-	-	23
	Schwannoma	-	-	-	10	-	-	10
NSE	GCT	-	-	3	20	-	-	23
	Schwannoma	-	4	6	-	-	-	10
SOX10	GCT	1	-	-	22	1	-	22
	Schwannoma	-	-	-	10	-	-	10
GAP43	GCT	-	-	2	21	-	-	23
	Schwannoma	-	-	4	6	-	3	7
HLA-DR	GCT	-	-	6	17	-	-	23
	Schwannoma	-	-	4	6	-	-	10
CD68	GCT	-	-	17	6	-	-	23
	Schwannoma	1	6	3	-	1	6	3
CD163	GCT *	22 *	-	-	-	22 *	-	-
	Schwannoma	-	-	1	9	-	-	10
CD40	GCT	23	-	-		23	-	-
	Schwannoma	10	-	-		10	-	-
CD11c	GCT	23	-	-		23	-	-
	Schwannoma	10	-	-		10	-	-

* Case 2 of GCT did not have a section for CD163 IHC.

For each antibody assessed, chi-squared tables were created using staining intensity as an ordinal x-variable and cell type as a nominal y-variable, with a Bonferroni correction applied to account for multiple testing. Staining scores for CD40, CD11c, and S100 were identical in GCTs and Schwannomas. No significant differences were found for SOX10 ($p = 0.5$), GAP43 ($p = 0.03$), or HLA-DR ($p = 0.4$), whereas NSE ($p = 0.000008$) and CD68 ($p = 0.0001$) exhibited higher intensity in GCTs, and CD163 was more strongly expressed in Schwannomas ($p = 0.00000007$).

A Cochrane-Armitage test comparing overall staining intensities across all markers confirmed a significant difference between GCTs and Schwannomas ($\alpha = 0.05$, $p = 0.000004$). Marker expression did not correlate with clinical features such as tumour size or location.

Digital Q-score analysis using QuPath identified positively stained cells, which were categorized into low, medium, and high intensity. H-score distributions suggested a non-Gaussian pattern, but the small sample size limited variance analysis. Both Student's t-test and Welch's t-test were applied, with a Bonferroni-adjusted significance threshold of 0.0125 ($\alpha\_bonferroni = 0.05/4$). H-score comparisons for GAP43, HLA-DR, CD68, and CD163 between GCTs and Schwannomas are shown in **Figure 3**.

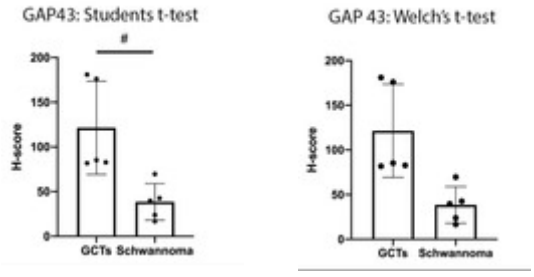

a) b)

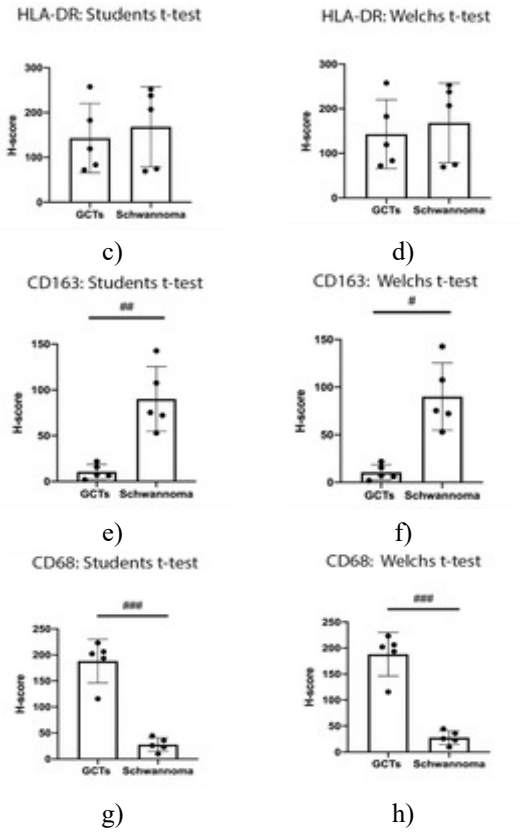

Figure 3. H-score comparisons between GCTs and Schwannomas for various antibodies. For GAP43, statistical analysis using Student's t-test (α = 0.0125) yielded p = 0.0108 (A), and Welch's t-test gave p = 0.0201 (B); significance threshold: # p ≤ 0.0125. For HLA-DR, Student's t-test (C) and Welch's t-test (D) both resulted in p = 0.646. For CD163, Student's t-test (E) showed p = 0.0012, and Welch's t-test (F) gave p = 0.0062; significance thresholds: # p ≤ 0.0125, ## p ≤ 0.005. For CD68, Student's t-test (G) gave p < 0.0001, and Welch's t-test (H) gave p = 0.0006; significance threshold: ### p ≤ 0.001.

H-scores obtained via digital analysis were compared with manually scored cell staining intensities using Pearson's correlation coefficient and t-tests for continuous variables. Results, summarized in **Table 3**, demonstrated an almost perfect correlation between manual scoring and QuPath-derived H-scores. A Bonferroni correction was not necessary because all p-values were extremely low.

Table 3. Summary of the comparison of cell stain intensity using manual semiquantitative scoring and H-score derived from QuPath.

Antibody	Correlation (r)	95% CI	p-Value
All tumours	0.906	0.827–0.949	0.00000000 0000001
GCTs only	0.903	0.767–0.961	0.00000005
Schwannomas only	0.9	0.759–0.960	0.00000007
GAP43	0.92	0.689–0.981	0.0002
HLA-DR	0.961	0.841–0.991	0.000009
CD68	0.989	0.951–0.997	0.00000007
CD163	0.979	0.911–0.979	0.0000008

Summary of Cq values from RT-qPCR

RT-qPCR was employed to assess mRNA expression, and the results are presented descriptively without statistical analysis. Six samples successfully amplified the housekeeping gene and were subsequently used to measure target gene expression. Cases 18 and 23 exhibited the lowest Cq values, indicating relatively higher expression levels, whereas Cases 1, 3, 8, and 15 displayed lower expression.

CD68 transcripts were detected in 5 of the 6 samples analyzed; Case 1 lacked detectable CD68 mRNA despite strong immunohistochemical staining in all granular cells. The remaining samples showed measurable CD68 expression.

Aside from Case 23 and the no-template control (NTC), no samples exhibited detectable expression of SOX2, SOX9, SOX10, NF2, or nestin. BTub3 expression was observed only in Cases 18 and 23, while all other samples were negative. SOX2 and GFAP mRNA were undetectable in all cases **(Tables 4 and 5)**.

Table 4. Summary of RNA concentration and B-actin and CD68 amplification cycles.

Case	RNA Concentration (µg/mL)	B-Actin Reactivity (Cq Value)	CD68 Reactivity (Cq Value)
1	6.5	34.70	-
3	17.4	37.38	37.15
6	4.24 *		
7	2.88 *		
8	5.7	36.94	35.96
15	7.4	34.53	37.12
16	Low *		
17	2.2 *		
18	10	29.71	32.53
22	4.16 *		
23	6.5	28.89	25.60
NTC		-	-

* = RNA concentration insufficient to proceed with RT-qPCR. - = no amplification.

Table 5. Summary of Cq values for Case 23.

Gene	Cq Value
CD68	29.60
Nestin	39.02
SOX2	-
SOX9	36.18
SOX10	38.01
NF2	37.14
GFAP	-
Beta Actin	28.89
Beta TUB3	36.72

- = no amplification.

GCTs are currently understood to originate from Schwann cells or to differentiate toward a Schwann cell phenotype [1], although other potential origins have been proposed, including myoblasts [1], fibroblasts [13], histiocytes [14], and endomesenchymal cells [9]. Evidence supporting Schwann cell differentiation includes the similarity of GCTs and Schwannomas in their immunohistochemical profiles for neural crest cell (NCC) and neuroectodermal markers such as SOX10, S100, and NSE.

GCTs and Schwannomas show marked differences in lysosomal marker CD68 expression: GCTs demonstrate strong, diffuse staining, whereas Schwannomas show weak staining in only a small subset of cells. CD68 positivity supports a potential antigen-presenting cell (APC) phenotype. The granular appearance of GCTs has been linked to lysosome accumulation, consistent with mutations in H^+-ATPase accessory protein genes ATP6AP1 and ATP6AP2, highlighting abnormal lysosomal content in granular cells [23]. These genetic findings suggest that GCTs are genuine neoplasms rather than reactive lesions.

Protein expression supporting an NCC origin of GCTs

Polyclonal S100 antibodies are widely used to help differentiate spindle cell lesions of NCC versus non-NCC origin, with the S100B isoform being highly specific. Neural and glial cells normally express high levels of S100, particularly S100B [44], and most benign and malignant NCC-derived tumours also express S100 [44]. However, S100 expression can be induced in a range of tumours from all germ layers, particularly under oxidative stress or inflammatory conditions, including S100A8, S100A9, S100A12, and S100B [45].

The strong nuclear staining observed with SOX10 provides further support for an NCC origin or differentiation and is increasingly recognized as a more specific NCC marker than S100. Interestingly, one case in this study lacked SOX10 immunoreactivity while showing strong S100 positivity. Repeat staining confirmed the absence of SOX10, and the tissue was retained for analysis. This absence may reflect loss of SOX10 during tumorigenesis or a technical artifact such as freezing during transport. Although SOX10 is expressed in nearly all benign peripheral nerve sheath tumours (BPNSTs), it is absent in approximately 30% of malignant peripheral nerve sheath tumours (MPNSTs), which can complicate pathological diagnosis [46]. No previous reports describe peripheral GCTs that are SOX10-negative but S100-positive. Interestingly, central nervous system GCTs, believed to arise from astrocytes, are SOX10-negative despite histologic similarity to peripheral GCTs [47]. Conversely, some GCTs have been reported as S100-negative but SOX10-positive, termed primitive GCTs, though it remains unclear whether these arise from a distinct NCC-derived mesenchymal lineage or have lost S100B expression [48].

Both GCTs and Schwannomas were positive for NSE, supporting an NCC origin. Notably, GCTs exhibited higher NSE staining intensity in a larger proportion of cells than Schwannomas, which may reflect higher metabolic activity. Previous studies have shown NSE upregulation in both NCC-derived and non-NCC tumours under conditions of inflammation or hypoxic stress [34, 49–51].

This study is the first to demonstrate GAP43 immunoreactivity in GCTs. GAP43 is a relatively newly identified protein considered highly specific for neural and glial tissues, though its function in glial cells is not fully understood. Evidence indicates it facilitates neurite extension during development and after nerve injury by promoting growth cone formation [36]. GAP43 is present in repair Schwann cells and Schwann cell precursors but absent in mature Schwann cells, appearing several weeks after nerve injury during Wallerian degeneration once myelin debris is cleared [7]. Unlike S100 and SOX10, GAP43 expression persists in MPNSTs and has been proposed to have higher sensitivity and specificity for NCC-derived spindle cell malignancies [52]. Additional studies have detected GAP43 in various cancers [53–55], suggesting it may have broader roles in tumorigenesis. Its presence in GCTs provides new evidence for a neural crest origin and supports the hypothesis that GCT granular cells resemble repair Schwann cells or precursors more than mature Schwann cells.

A further novel observation concerns the distribution of GAP43 in Schwannomas. High-intensity staining was observed in the cellular Antoni A regions, while the less dense Antoni B regions exhibited low staining in fewer than half of the spindle cells. Antoni B areas

are typically considered degenerative zones, characterized by fibrosis, hyalinisation, mucin deposition, thrombosis, and infiltration by macrophages and lymphocytes [56, 57]. This pattern suggests that GAP43 expression decreases as Schwannoma cells transition from Antoni A to Antoni B areas, and indicates that GCT granular cells are more comparable to the spindle cells in Antoni A regions than those in Antoni B regions.

Protein expression suggesting an APC phenotype

Overall, the findings of this study provide only limited support for an antigen-presenting cell (APC) phenotype in GCTs. At the start of the investigation, the functional significance of the abundant lysosomes in granular cells was unclear, and it remained uncertain whether GCTs were reactive lesions or true neoplasms. Consistent with previous reports, strong CD68 staining was observed in most granular cells, confirming that the granules are lysosomes. CD68 is widely recognized as a marker for phagocytic cells, including histiocytes, monocytes, giant cells, Kupffer cells, and osteoclasts, with its expression regulated by a macrophage-specific promoter gene [26, 27]. It had been hypothesized that lysosomes in GCTs might indicate a phagocytic role following nerve injury.

The work of Pareja *et al*. has since clarified that the accumulation of lysosomes in GCTs results from mutations in ATP6AP1 and ATP6AP2, which encode V-ATPase accessory proteins involved in endosome acidification and transport [23]. This provides a genetic explanation for the strong CD68 immunoreactivity, demonstrating that lysosome accumulation reflects altered lysosomal function rather than a phagocytic activity. HLA-DR immunoreactivity also showed strong staining in GCTs. HLA-DR is typically associated with APCs, including B cells, activated T cells, and professional APCs such as monocytes, macrophages, and dendritic cells [24]. Initially, it was hypothesized that HLA-DR in combination with CD68 could indicate an antigen-presenting role for GCTs; however, the non-functional lysosomes and lack of CD40 expression argue against T-cell activation capacity [58].

Alternative explanations for HLA-DR expression in GCTs include a role analogous to that in melanomas, where HLA-DR is linked to tumor antigen presentation, tissue inflammation, and anti-tumor immune responses, serving as a positive prognostic marker [59]. Another possibility is that HLA-DR reflects epithelial–mesenchymal transformation, indicating tissue dedifferentiation rather than genuine APC function. Finally, HLA-DR expression could simply reflect tissue inflammation, as it has been observed in various cell types during inflammatory responses [60–62]. Interestingly, all Schwannomas in this study were HLA-DR-positive, a novel observation for this tumour type; HLA-DR expression has previously been reported in gliomas and neuroblastomas, where it is associated with increased tumor inflammation and poorer outcomes [63].

GCTs were negative for CD163, CD40, and CD11c, providing no further support for an APC phenotype. An unexpected finding was the strong CD163 immunoreactivity in Schwannomas, which may reflect a spindle cell phenotype resembling phagocytic repair Schwann cells or indicate an inflammatory process. In GCTs, some dendritic-appearing cells expressed CD163, suggesting localized inflammation that could explain HLA-DR positivity but does not substantiate an APC phenotype.

Interpretation of RT-qPCR data

Unexpectedly, SOX10 mRNA was detected in only one of six GCT cases (Case 23), with the remaining five showing no amplification, which conflicts with prior studies reporting consistent SOX10 immunoreactivity and with the IHC results from this study. Although RT-qPCR is generally considered more sensitive and precise than IHC, this discrepancy may be explained by the stability of SOX10 protein, which may require only minimal mRNA levels to maintain cellular function, potentially falling below detection limits over 40 PCR cycles. Alternatively, SOX10 mRNA might be more prone to degradation than CD68 or beta-actin, so despite adequate RNA concentrations measured via Qubit, the transcripts could have been fragmented. It is also possible that both very low mRNA abundance and partial degradation contributed. Without detectable SOX10 transcripts, drawing conclusions regarding nestin, SOX2, SOX9, SOX10, NF2, and GFAP expression is challenging.

Study limitations

While digital quantification improves accuracy and sensitivity compared with manual scoring, whole-slide analysis using QuPath faces challenges, including the manual adjustment of parameters and accurate delineation of nuclei, cytoplasm, and cell boundaries. Given the strong immunohistochemical evidence for SOX10 in GCTs, the lack of amplification is interpreted as likely due to RNA quality issues rather than true absence of expression.

Future directions

Future studies should consider alternative RNA extraction methods to investigate the neural crest cell

developmental phenotype in GCTs. Additional research is warranted to characterize the range of granular lesions, including potential mutations affecting lysosome biogenesis, acidification, and transport, using sequencing approaches similar to those applied to identify ATP6AP1 and ATP6AP2 mutations in GCTs.

Materials and Methods

Case selection

Archived FFPE tissues from 23 consecutive benign GCTs and 10 schwannomas (2006–2016) were retrieved from the Department of Pathology, Schulich School of Medicine and Dentistry, Western University. No malignant cases were included. Patient data, including age, sex, and lesion location, were collected **(Table 1)**.

Immunohistochemistry (IHC)

Neural markers (S100, SOX10, NSE, GAP43) and APC markers (HLA-DR, CD68, CD163, CD40, CD11c) were analyzed as listed in **Table 6**. Five-micron sections were cut from hydrated FFPE blocks. Automated IHC staining for S100, SOX10, NSE, HLA-DR, CD68, and CD163 antibodies was performed using the Dako Autostainer Link 48, with each run including a standard positive tissue array and at least one negative control per tumor type.

Table 6. Summary of the antibodies used for immunohistochemistry of GCTs and schwannomas.

Antibody	Manufacture/Cat Number	Antibody Type	Constituent Tissue and Labelling Targets	Dilution
S100	Dako, Santa Clara CA IR50461-2	Rabbit polyclonal	Neural tissues, S100B (strong) S100A1 and S100A6 (weak)	Automated
NSE	Dako, Santa Clara CA IR61261-2	Mouse monoclonal	Neural tissues, γ-enolase subunit	Automated
SOX10	Santa Cruz Biotech, Dallas TX, sc-365692	Mouse monoclonal	Neural tissues, SOX10 transcription factor	Automated
GAP43	Bio-Techne Canada, Oakville On, NB300-143	Rabbit polyclonal	Regenerating neural tissues/growth cones, GAP43 intracellular growth protein/membrane protein	1/5000
HLA-DR	Dako, Santa Clara CA MO74601	Mouse monoclonal	APCs and lymphocytes, Alpha-chain of HLA-DR cell surface receptor	Automated
CD68	Dako, Santa Clara CA GA61361-2	Mouse monoclonal	Macrophage, lysosomal-associated membrane proteins	Automated
CD163	Vector laboratories, Burlingame CA VP-C374	Mouse monoclonal	Macrophage, hemoglobin-scavenger receptor	Automated
CD40	Abcam, Toronto ON, ab13545	Rabbit polyclonal	APCs, cell surface innate immune response costimulatory protein	1/1000
CD11c	Abcam, Toronto ON, ab52632	Rabbit monoclonal	APCs, cell surface fibrinogen receptor	1/300

For the immunohistochemical procedure, sections from GCTs and schwannomas were used alongside appropriate positive controls—schwannomas for GAP43 and tonsils for CD40 and CD11c—and negative controls. Antigen retrieval was performed in a citrate buffer at pH 6 using a decloaking chamber (Biocare Medical, Pacheco, CA, USA). After cooling, the sections were washed with phosphate-buffered saline (PBS), placed in a humidified chamber, and blocked with 2.5% horse serum for 30 minutes. Primary antibodies were then applied: rabbit anti-human GAP43 (1:5000, NB300-143, Bio-Techne Canada, Oakville, ON), rabbit anti-human CD40 (1:1000, ab13545, Abcam, Toronto, ON), and rabbit anti-human CD11c (1:300, ab52632, Abcam, Toronto, ON), and incubated overnight at 4 °C with negative control slides.

The following day, sections were rinsed and treated with secondary antibodies. GAP43 and CD40 slides were incubated with immPRESS anti-rabbit IgG (VECTMP540150, MJS Biolynx, Brockville, ON) at room temperature for 30 minutes, while CD11c slides were incubated using the VECTASTAIN Elite ABC-HRP Kit (PK-7200, Vector Laboratories, Burlington, ON) under the same conditions. Visualization was achieved using a DAB peroxidase substrate kit (VECTSK4100, MJS Biolynx, Brockville, ON), and all slides were counterstained with Harris hematoxylin (Leica Biosystems, Concord, ON).

Assessment of immunostaining

Slides were evaluated under light microscopy and scored via semiquantitative methods. Additionally, five randomly selected cases of GCTs and schwannomas were digitally analyzed for GAP43, CD68, HLA-DR, and CD163 using QuPath (v0.1.2), an open-source platform validated for accurate and reproducible bioimage analysis [64, 65], accessible at https://qupath.github.io/ (accessed 1 June 2020).

Manual scoring

Manual evaluation focused on the large polygonal granular cells in GCTs and tumor cells within the capsule for schwannomas. Staining intensity was assessed relative to positive controls using the following scale: 0 = negative, 1 = weak, 2 = moderate, 3 = strong. The proportion of stained cells was categorized as 0 = 0%, 1 = 0–50%, and 2 = >50%.

Digital analysis

High-resolution whole-slide images were captured for five GCT and five schwannoma cases stained for GAP43, HLA-DR, CD163, and CD68. Images for the same antibody were grouped into multi-slide projects in QuPath. Automated detection of cell nuclei relied on hematoxylin optical density and size criteria, while positive staining was determined by mean DAB optical density. A detection classifier was trained by visually selecting representative cells for low, medium, and high intensity. Outcomes were expressed as both the percentage of positive cells and as H-scores, calculated as: H-score = (3 × % strong) + (2 × % moderate) + (1 × % weak), ranging from 0 to 300.

RT-qPCR protocol

RNA was extracted from FFPE tissue blocks of GCTs, and complementary DNA (cDNA) was synthesized for the detection of CD68, nestin, SOX2, SOX9, SOX10, NF2, GFAP, beta-actin, and B-Tub3.

Tissue selection and preparation

Eleven FFPE blocks were identified as having sufficient tumor volume for RNA extraction. Corresponding H&E-stained slides were examined under light microscopy to locate areas representative of GCTs, avoiding non-tumor tissue. A 1 mm-diameter punch biopsy was taken from each block at a depth of 1 mm and collected in 1.5 mL tubes. To confirm the representativeness of the biopsy, 5 µm sections from the FFPE blocks were H&E-stained and visually inspected under a microscope, verifying that the punch samples consisted solely of tumor tissue in all 11 cases.

RNA extraction

Deparaffinization of the tissue plugs was performed, followed by RNA isolation using the High Pure FFPE RNA Micro Kit (Roche, Mannheim, Germany; Cat. No. 04823125001). Tissue plugs were incubated with lysis buffer containing 10% SDS and proteinase K at 55 °C for 3 hours. The lysates were applied to RNA-binding spin columns and centrifuged, discarding flow-through. DNase treatment was performed for 15 minutes at room temperature to remove genomic DNA. RNA was then purified through sequential washes with buffer solutions, each followed by centrifugation at 8,000 × g for 5 minutes, discarding the supernatant. RNA was finally eluted with buffer and collected by centrifugation at 8,000 × g for 1 minute for downstream quantification.

RNA quantification

RNA concentrations were measured using the Qubit Quan-iT RNA BR Assay Kit (Thermo Fisher Scientific, Carlsbad, CA, USA; Cat. No. Q10210) and a Qubit fluorometer. The Qubit reagent was diluted 1:200 in buffer, and 198 µL of working solution was combined with 2 µL of RNA in 0.5 mL tubes. Calibration was performed using two Qubit standards prepared with 10 µL standard and 190 µL working solution. RNA concentrations were calculated using the formula: RNA concentration = QF × (200/x), with QF representing the fluorometer reading and x the sample volume in µL.

cDNA synthesis and RT-qPCR

Six of the eleven samples yielded sufficient RNA for cDNA synthesis. Reverse transcription was performed using the iScript cDNA Synthesis Kit (Bio-Rad, Hercules, CA, USA; Cat. No. 1708890). For each reaction, a 20 µL mixture was prepared containing 4 µL 5× iScript reaction mix with reverse transcriptase, 100 ng RNA, and nuclease-free water to volume. RT-qPCR reactions were set up in 96-well plates (Hard-Shell® Low-Profile Thin-Wall, Bio-Rad, HSP-9601), with each well containing 10 µL RT2 SYBR Green qPCR Mastermix (Bio-Rad, 330501), 2 µL primers, 1 µL cDNA, and 7 µL nuclease-free water. No-template controls (NTCs) included 8 µL nuclease-free water in place of cDNA. Arrays were organized by case number on the y-axis, and amplification was performed for 40 cycles using the CFX Connect system (Bio-Rad, Mississauga, ON, Canada). Details of primers and assay conditions are provided in **Table 7**.

Table 7. Summary of primers employed in RT-qPCR.

Gene Assay	Vendor	Cat Number	Amplicon Length	Exon-Spanning
CD68	QIAGEN	QT00037184	73 bp	Y
NESTIN	QIAGEN	QT01015301	75 bp	Y
SOX2	QIAGEN	QT00237601	64 bp	N
SOX9	QIAGEN	QT00001498	111 bp	Y
SOX10	QIAGEN	QT01670326	145 bp	Y
NF2	QIAGEN	QT00030191	148 bp	Y
GFAP	QIAGEN	QT00081151	96 bp	Y
Beta-Actin	QIAGEN	QT01680476	104 bp	Y
Beta-TUB3	QIAGEN	QT00083713	78 bp	Y

Statistical analysis

Since both the percentage of cells stained and staining intensity are ordinal variables, a linear-by-linear association test was performed to evaluate the correlation between these two parameters across the combined GCT and schwannoma data, revealing an almost perfect correlation. Due to this strong association, subsequent analyses focused solely on staining intensity, with findings inferred to reflect the proportion of positive cells. To compare overall staining intensities between GCTs and schwannomas for the nine IHC markers, a Cochrane-Armitage trend test using a generalized chi-squared approach was applied, treating intensity as an ordered variable and cell type as a nominal variable. A Bonferroni correction was implemented to account for multiple testing. Three markers—S100, CD40, and CD11c—showed no variation between GCTs and schwannomas and were therefore excluded from the Bonferroni calculation, yielding m=6 and αBonferroni=0.5/6.

For the digital analysis data, comparisons of H-scores between GCTs and schwannomas were performed using both Student's t-test and Welch's t-test, with a Bonferroni adjustment applied for m=4tests (αBonferroni=0.5/4). Pearson correlation coefficients were calculated to evaluate the relationship between H-scores and manual staining intensity for each antibody.

Conclusion

The findings of this study reinforce the concept that GCTs likely originate from neural crest cells, most plausibly along the Schwann cell lineage, as supported by significant GAP43 immunoreactivity alongside S100, SOX10, and NSE expression. The presence of HLA-DR and CD68 indicates induction of an antigen-presenting cell-like phenotype in this peripheral nerve sheath tumor. Based on the accumulated immunophenotypic evidence, we propose that GCTs be formally classified within the peripheral nerve sheath tumor category. The designation "granular cell nerve sheath tumor" may better reflect the nature of this rare entity, and we recommend that diagnostic workup includes a comprehensive immunohistochemical and molecular panel, incorporating markers such as GAP43.

Acknowledgments: None

Conflict of Interest: None

Financial Support: None

Ethics Statement: None

References

1. Ordóñez NG, Mackay B. Granular cell tumor: a review of the pathology and histogenesis. Ultrastruct Pathol. 1999;23(3):207–22.
2. Allon I, Kaplan I, Gal G, Chaushu G, Allon DM. The clinical characteristics of benign oral mucosal tumors. Med Oral Patol Oral Cir Bucal. 2014;19(5):e438–43.
3. Speight PM. World Health Organization classification of tumors: Pathology and genetics of head and neck tumors. In: Barnes L, Everson J, Reichart P, Sidransky D, editors. Lyon: IARC Press; 2005.
4. Goodstein ML, Eisele DW, Hyams VJ, Kashima HK. Multiple synchronous granular cell tumors of the upper aerodigestive tract. Otolaryngol Head Neck Surg. 1990;103(4):664–8.
5. Barakat M, Kar AA, Pourshahid S, Ainechi S, Lee HJ, Othman M, et al. Gastrointestinal and biliary granular cell tumor: Diagnosis and management. Ann Gastroenterol. 2018;31(4):439–47.

6. Porta N, Mazzitelli R, Cacciotti J, Cirenza M, Labate A, Lo Schiavo MG, et al. A case report of a rare intramuscular granular cell tumor. Diagn Pathol. 2015;10(1):162.
7. Curtis R, Stewart HJS, Hall SM, Wilkin GP, Mirsky R, Jessen KR. GAP-43 is expressed by nonmyelin-forming Schwann cells of the peripheral nervous system. J Cell Biol. 1992;116(6):1455–64.
8. Rivlin ME, Meeks GR, Ghafar MA, Lewin JR. Vulvar granular cell tumor. World J Clin Cases. 2013;1(5):149–51.
9. Gurzu S, Ciortea D, Tamasi A, Golea M, Bodi A, Sahlean DI, et al. The immunohistochemical profile of granular cell (Abrikossoff) tumor suggests an endomesenchymal origin. Arch Dermatol Res. 2015;307(2):151–7.
10. Lack EE, Worsham RGF, Callihan MD, Crawford BE, Klappenbach S, Rowden G, et al. Granular cell tumor: a clinicopathologic study of 110 patients. J Surg Oncol. 1980;13(4):301–16.
11. Worsaae N, Schwartz O, Pindborg JJ. Follow-up study of 14 oral granular cell tumors. Int J Oral Surg. 1979;8(2):133–9.
12. Ferreira JCB, Oton-Leite AF, Guidi R, Mendonça EF. Granular cell tumor mimicking a squamous cell carcinoma of the tongue: a case report. BMC Res Notes. 2017;10(1):1–6.
13. Miller AS, Leifer C, Chen SY, Harwick RD. Oral granular-cell tumors: Report of twenty-five cases with electron microscopy. Oral Surg Oral Med Oral Pathol. 1977;44(2):227–37.
14. Sobel HJ, Marquet E, Avrin E, Schwarz R. Granular cell myoblastoma: an electron microscopic and cytochemical study illustrating the genesis of granules and aging of myoblastoma cells. Am J Pathol. 1971;65(1):59–78.
15. Manara GC, De Panfilis G, Bacchi AB, Ferrari C, Tedeschi F, Brusati R, et al. Fine structure of granular cell tumor of Abrikossoff. J Cutan Pathol. 1981;8(4):277–82.
16. Stewart CM, Watson RE, Eversole LR, Fischlschweiger W, Leider AS. Oral granular cell tumors: a clinicopathologic and immunocytochemical study. Oral Surg Oral Med Oral Pathol. 1988;65(4):427–35.
17. Mukai M. Immunohistochemical localization of S-100 protein and peripheral nerve myelin proteins (P2 protein, P0 protein) in granular cell tumors. Am J Pathol. 1983;112(2):139–45.
18. Musha A, Ogawa M, Yokoo S. Granular cell tumors of the tongue: Fibroma or schwannoma? Head Face Med. 2018;14(1):1–5.
19. Campbell LK, Thomas JR, Lamps LW, Smoller BR, Folpe AL. Protein gene product 9.5 (PGP 9.5) is not a specific marker of neural and nerve sheath tumors: An immunohistochemical study of 95 mesenchymal neoplasms. Mod Pathol. 2003;16(10):963–9.
20. Martins MD, De Jesus LA, Fernandes KPS, Bussadori SK, Taghloubi SA, Martins MAT. Intra-oral schwannoma: case report and literature review. Indian J Dent Res. 2009;20(1):121–5.
21. Shintaku M. Immunohistochemical localization of autophagosomal membrane-associated protein LC3 in granular cell tumor and schwannoma. Virchows Arch. 2011;459(3):315–9.
22. Regezi JA, Zarbo RJ, Courtney RM, Crissman JD. Immunoreactivity of granular cell lesions of skin, mucosa, and jaw. Cancer. 1989;64(7):1455–60.
23. Pareja F, Brandes AH, Basili T, Selenica P, Geyer FC, Fan D, et al. Loss-of-function mutations in ATP6AP1 and ATP6AP2 in granular cell tumors. Nat Commun. 2018;9(1):3533.
24. Choo SY. The HLA system: genetics, immunology, clinical testing, and clinical implications. Yonsei Med J. 2007;48(1):11–23.
25. Bergstrom RT, Silverman DA, Chambers K, Kim JA. CD40 monoclonal antibody activation of antigen-presenting cells improves therapeutic efficacy of tumor-specific T cells. Otolaryngol Head Neck Surg. 2004;130(1):94–103.
26. Chistiakov DA, Killingsworth MC, Myasoedova VA, Orekhov AN, Bobryshev YV. CD68/macrosialin: not just a histochemical marker. Lab Invest. 2017;97(1):4–13.
27. Gottfried E, Kunz-Schughart LA, Weber A, Rehli M, Peuker A, Müller A, et al. Expression of CD68 in non-myeloid cell types. Scand J Immunol. 2008;67(5):453–63.
28. Etzerodt A, Moestrup SK. CD163 and inflammation: biological, diagnostic, and therapeutic aspects. Antioxid Redox Signal. 2013;18(17):2352–63.
29. Chatzigeorgiou A, Lyberi M, Chatzilymperis G, Nezos A, Kamper E. CD40/CD40L signaling and its implication in health and disease. Biofactors. 2009;35(6):474–83.
30. Wu J, Wu H, An J, Ballantyne CM, Cyster JG. Critical role of integrin CD11c in splenic dendritic cell capture of missing-self CD47 cells to induce adaptive immunity. Proc Natl Acad Sci U S A. 2018;115(26):6786–91.
31. Male DK. Immunology. 8th ed. Amsterdam: Elsevier; 2013. ISBN: 978-0-7020-5028-2.

32. Surbhi S, Metgud R, Naik S, Patel S. Spindle cell lesions: a review on immunohistochemical markers. J Cancer Res Ther. 2017;13(3):412–8.
33. Karamchandani JR, Nielsen TO, van de Rijn M, West RB. Sox10 and S100 in the diagnosis of soft-tissue neoplasms. Appl Immunohistochem Mol Morphol. 2012;20(5):445–50.
34. Isgrò MA, Bottoni P, Scatena R. Neuron-specific enolase as a biomarker: biochemical and clinical aspects. Adv Exp Med Biol. 2015;867:125–43.
35. Perrone-Bizzozero NI, Neve RL, Irwin N, Lewis S, Fischer I, Benowitz LI. Post-transcriptional regulation of GAP-43 mRNA levels during neuronal differentiation and nerve regeneration. Mol Cell Neurosci. 1991;2(5):402–9.
36. Denny J. Molecular mechanisms, biological actions, and neuropharmacology of the growth-associated protein GAP-43. Curr Neuropharmacol. 2006;4(4):293–304.
37. Rizzino A. Sox2 and Oct-3/4: A versatile pair of master regulators that orchestrate the self-renewal and pluripotency of embryonic stem cells. Wiley Interdiscip Rev Syst Biol Med. 2009;1(2):228–36.
38. Jo A, Denduluri S, Zhang B, Wang Z, Yin L, Yan Z, et al. The versatile functions of Sox9 in development, stem cells, and human diseases. Genes Dis. 2014;1(2):149–61.
39. Michalczyk K, Ziman M. Nestin structure and predicted function in cellular cytoskeletal organisation. Histol Histopathol. 2005;20(2):665–71.
40. Erinanç H, Göktürk HS, Kanat Ünler G, Karagülle E. Utility of Nestin immunohistochemistry in the diagnosis of granular cell tumor. Arch Clin Exp Med. 2018;3(4):160–4.
41. Kim HS, Lee J, Lee DY, Kim YD, Kim JY, Lim HJ, et al. Schwann cell precursors from human pluripotent stem cells as a potential therapeutic target for myelin repair. Stem Cell Rep. 2017;8(6):1714–26.
42. Katsetos CD, Del Valle L, Geddes JF, Aldape K, Boyd JC, Legido A, et al. Localization of the neuronal class III β-tubulin in oligodendrogliomas: Comparison with Ki-67 proliferative index and 1p/19q status. J Neuropathol Exp Neurol. 2002;61(4):307–20.
43. Lebok P, Öztürk M, Heilenkötter U, Jaenicke F, Müller V, Paluchowski P, et al. High levels of class III β-tubulin expression are associated with aggressive tumor features in breast cancer. Oncol Lett. 2016;11(3):1987–94.
44. Kuberappa PH, Bagalad BS, Ananthaneni A, Kiresur MA, Srinivas GV. Certainty of S100 from physiology to pathology. J Clin Diagn Res. 2016;10(2):ZE10–5.
45. Donato R, Cannon BR, Sorci G, Riuzzi F, Hsu K, Weber DJ, et al. Functions of S100 proteins. Curr Mol Med. 2013;13(1):24–57.
46. Kang Y, Pekmezci M, Folpe AL, Ersen A, Horvai AE. Diagnostic utility of SOX10 to distinguish malignant peripheral nerve sheath tumor from synovial sarcoma, including intraneural synovial sarcoma. Mod Pathol. 2014;27(1):55–61.
47. Wisell J, Kleinschmidt-DeMasters BK. Sox10 nuclear immunostaining lacks diagnostic utility for CNS granular cell tumors. J Neuropathol Exp Neurol. 2014;73(2):98–100.
48. Solomon LW. S-100 negative granular cell tumor of the oral cavity. Head Neck Pathol. 2018;10(3):367–73.
49. Roberts SL, Dun XP, Doddrell RDS, Mindos T, Drake LK, Onaitis MW, et al. Sox2 expression in Schwann cells inhibits myelination in vivo and induces influx of macrophages to the nerve. Development. 2017;144(17):3114–25.
50. Vinores SA, Herman MM, Rubinstein LJ. Electron-immunocytochemical localization of neuron-specific enolase in cytoplasm and on membranes of primary and metastatic cerebral tumours and on glial filaments of glioma cells. Histopathology. 1986;10(8):891–908.
51. Mjønes P, Sagatun L, Nordrum IS, Waldum HL. Neuron-specific enolase as an immunohistochemical marker is better than its reputation. J Histochem Cytochem. 2017;65(11):687–703.
52. Chen W, Chen P, Lu D, Lind AC, Dehner LP. Growth-associated protein 43 in differentiating peripheral nerve sheath tumors from other non-neural spindle cell neoplasms. Mod Pathol. 2014;27(2):184–93.
53. Zheng C, Quan RD, Wu CY, Hu J, Lin BY, Dong XB, et al. Growth-associated protein 43 promotes thyroid cancer cell lines progression via epithelial-mesenchymal transition. J Cell Mol Med. 2019;23(11):7974–84.
54. Zhang F, Jin J, Wu J, Chen K, Huang M, Yu H, et al. Abstract 1083: GAP43, a novel potential metastases promoter in non-small cell lung cancer. Cancer Res. 2018;78(13 Suppl):1083.
55. Klein A, Olendrowitz C, Schmutzler R, Hampl J, Schlag PM, Maass N, et al. Identification of brain- and bone-specific breast cancer metastasis genes. Cancer Lett. 2009;276(2):212–20.
56. Wippold FJ, Lubner M, Perrin RJ, Lämmle M, Perry A. Neuropathology for the neuroradiologist:

Antoni A and Antoni B tissue patterns. AJNR Am J Neuroradiol. 2007;28(9):1633–8.
57. Papiez J, Rojiani MV, Rojiani AM. Vascular alterations in schwannoma. Int J Clin Exp Pathol. 2014;7(7):4032–8.
58. Kurtin PJ, Bonin DM. Immunohistochemical demonstration of the lysosome-associated glycoprotein CD68 (KP-1) in granular cell tumors and schwannomas. Hum Pathol. 1994;25(11):1172–8.
59. Chen YY, Chang WA, Lin ES, Chen YJ, Kuo PL. Expressions of HLA class II genes in cutaneous melanoma were associated with clinical outcome: Bioinformatics approaches and systematic analysis of public microarray and RNA-Seq datasets. Diagnostics (Basel). 2019;9(2):59.
60. Mehrfeld C, Zenner S, Kornek M, Lukacs-Kornek V. The contribution of non-professional antigen-presenting cells to immunity and tolerance in the liver. Front Immunol. 2018;9:635.
61. Wosen JE, Mukhopadhyay D, Macaubas C, Mellins ED. Epithelial MHC class II expression and its role in antigen presentation in the gastrointestinal and respiratory tracts. Front Immunol. 2018;9:2144.
62. Epstein SP, Gadaria-Rathod N, Wei Y, Maguire MG, Asbell PA. HLA-DR expression as a biomarker of inflammation for multicenter clinical trials of ocular surface disease. Exp Eye Res. 2013;111:95–104.
63. de Muralt B, de Tribolet N, Diserens AC, Stavrou D, Mach JP, Carrel S. Phenotyping of 60 cultured human gliomas and 34 other neuroectodermal tumors by means of monoclonal antibodies against glioma, melanoma and HLA-DR antigens. Eur J Cancer Clin Oncol. 1985;21(2):204–16.
64. Bankhead P, Loughrey MB, Fernández JA, Dombrowski Y, McArt DG, Dunne PD, et al. QuPath: Open source software for digital pathology image analysis. Sci Rep. 2017;7(1):16878.
65. Loughrey MB, Bankhead P, Coleman HG, Hagan RS, Craig S, McCorry AMB, et al. Validation of the systematic scoring of immunohistochemically stained tumour tissue microarrays using QuPath digital image analysis. Histopathology. 2018;73(2):327–38.